Journal of Environmental Chemical Engineering 10 (2022) 108448

Contents lists available at ScienceDirect

Journal of Environmental Chemical Engineering

journal homepage: www.elsevier.com/locate/jece

U(VI) binding onto electrospun polymers functionalized with phosphonate surfactants

Nabil Shaikh [a], Jiajie Qian [b], Sewoon Kim [b], Hoa Phan [c], Juan S. Lezama-Pacheco [d], Abdul-Mehdi S. Ali [e], David M. Cwiertny [b], Tori Z. Forbes [c], Amanda J. Haes [c], José M. Cerrato [a,*]

[a] Department of Civil, Construction, & Environmental Engineering, University of New Mexico, MSC01 1070, Albuquerque, NM 87131, USA
[b] Department of Civil and Environmental Engineering, University of Iowa, Iowa City IA52242, USA
[c] Department of Chemistry, University of Iowa, Iowa City, IA 52242, USA
[d] Department of Environmental Earth System Science, Stanford University, Stanford, CA 94305, USA
[e] Department of Earth and Planetary Sciences, University of New Mexico, MSC03 2040, Albuquerque, NM 87131, USA

ARTICLE INFO

Editor: Yunho Lee

Keywords:
Phosphonate
Electrospun polymer
Uranium
Spectroscopy
Sensing

ABSTRACT

We previously observed that phosphonate functionalized electrospun nanofibers can uptake U(VI), making them promising materials for sensing and water treatment applications. Here, we investigate the optimal fabrication of these materials and their mechanism of U(VI) binding under the influence of environmentally relevant ions (e.g., Ca^{2+} and CO_3^{2-}). We found that U(VI) uptake was greatest on polyacrylonitrile (PAN) functionalized with longer-chain phosphonate surfactants (e.g., hexa- and octadecyl phosphonate; HDPA and ODPA, respectively), which were better retained in the nanofiber after surface segregation. Subsequent uptake experiments to better understand specific solid-liquid interfacial interactions were carried out using 5 mg of HDPA-functionalized PAN mats with 10 μM U at pH 6.8 in four systems with different combinations of solutions containing 5 mM calcium (Ca^{2+}) and 5 mM bicarbonate (HCO_3^-). U uptake was similar in control solutions containing no Ca^{2+} and HCO_3^- (resulting in 19 ± 3% U uptake), and in those containing only 5 mM Ca^{2+} (resulting in 20 ± 3% U uptake). A decrease in U uptake (10 ± 4% U uptake) was observed in experiments with HCO_3^-, indicating that UO_2-CO_3 complexes may increase uranium solubility. Results from shell-by-shell EXAFS fitting, aqueous extractions, and surface-enhanced Raman scattering (SERS) indicate that U is bound to phosphonate as a monodentate inner sphere surface complex to one of the hydroxyls in the phosphonate functional groups. New knowledge derived from this study on material fabrication and solid-liquid interfacial interactions will help to advance technologies for use in the in-situ detection and treatment of U in water.

1. Introduction

The transport of U(VI) caused by natural and anthropogenic processes can be concerning for surrounding communities and ecosystems [1,2] due to the toxicological effects of U in humans, such as cancer and kidney failure. [2,3] For water treatment applications, selective U uptake is possible by chelation with organic functional groups (e.g. phosphonate, quaternary ammonia, etc.) embedded in the surface of solid substrates. [4,5] In particular, previous studies show up to three-fold increase in U uptake on phosphonate functionalized resins when compared to unfunctionalized materials, but the specific mechanisms affecting the solid-liquid interfacial interactions are not well understood. [6–8] Thus, fundamental understanding of U binding with phosphonate-functionalized materials is necessary for improving environmental remediation applications.

As a sorbent technology, electrospun polymers are ideal for promoting interfacial interactions due to their high surface to volume ratio and high porosity. Recent applications of electrospun polymers include passive sampling devices, materials for solid phase extraction, reactive filtration media, and platforms to concentrate dissolved targets for sensing applications. [9–15] PAN (polyacrylonitrile) is a common electrospun polymer with limited metal binding affinity via nitrile groups. [16–20] Uptake of U on PAN nanofibers can be enhanced by incorporating scavenging functional groups. In particular, phosphonates are an important chelating agent for U uptake due to strong binding over a wide pH range. [21–24] For example, we have previously shown that

* Corresponding author.
E-mail address: jcerrato@unm.edu (J.M. Cerrato).

https://doi.org/10.1016/j.jece.2022.108448
Received 12 May 2022; Received in revised form 11 August 2022; Accepted 13 August 2022
Available online 17 August 2022

electrospun PAN nanofibers can be functionalized to improve U adsorption by simply incorporating surfactants with a phosphonate head group [e.g., hexadecylphosphonate (HDPA)] directly into the sol-gel solution. [9,25] This approach exploits the recognized ability of certain surfactants to surface segregate during electrospinning, a process that results in the migration of the charged head of the surfactant to the polymer-air interface so as to minimize the free energy of interaction between the surfactant and the polymer support. [26] This produces PAN nanofibers that are surface-enriched in HDPA binding sites that are suitable for U uptake under environmentally relevant conditions.

With the development of such functionalized materials for potential use in U treatment and/or sensing, there remains a need to elucidate the nature of species formed when U binds to surface-immobilized phosphonate moieties, particularly under conditions relevant to the intended application of the material. Although investigations with phosphonate-functionalized materials in complex, environmentally relevant aquatic matrixes remain limited, there are extensive studies that have considered the interaction of U with phosphonate ligands in solution that may prove helpful in understanding U uptake in heterogeneous systems. [4,27,28] For example, computational chemistry studies using thermodynamics and quantum mechanical calculations have shown that binding of uranyl with aqueous phosphonate functional groups can occur as monodentate (UO_2-PO-) or binuclear bidentate (-PO-UO_2-PO-) surface complexes, even in the presence of competing ligands such as inorganic carbonate and phosphate anions. [27,29–31] For water treatment applications, carbonate is likely to be an important natural complexing agent that can react with U to form stable UO_2-CO_3 aqueous complexes. [30,32] Additionally, the presence of ternary U complexes involving a uranyl cation, carbonate anion, and alkaline earth metals like calcium (Ca) can influence the aqueous U(VI) speciation under circumneutral to alkaline pH conditions. [7,33,34] The presence of soluble calcium ions in the mM range, which is typical of hard water, can also promote adsorption of phosphonate onto a model solid surface. [35,36].

In this study, we expand upon our prior work with phosphonate-functionalized PAN nanofibers [25] to (i) optimize their synthesis with surface-segregating phosphonate surfactants to promote U uptake and (ii) elucidate via spectroscopic methods the exact nature of the U species bound by surface-phosphonate moieties under conditions more representative of water treatment and sensing applications. Phosphonate surfactants are available with a range of alkyl chain lengths (from 10 to 18 carbon units), which we anticipate will affect both the extent of surface segregation and the retention of the surfactant in PAN. Accordingly, we first established the influence of alkyl chain length on U uptake in batch systems complemented by surface spectroscopic characterization (i.e., X-ray photoelectron spectroscopy). Then, through a series of batch uptake experiments in solutions containing calcium (Ca^{2+}) and carbonate (CO_3^{2-}) ions followed by selective chemical extraction of different bound U species, we probed changes in U binding mechanisms on phosphonate-functionalized PAN nanofibers using a suite of spectroscopic techniques (X-ray Photoelectron Spectroscopy, X-ray Absorption Spectroscopy, Raman Spectroscopy).

This study builds upon our prior work where such functionalized nanofiber materials have been used to concentrate dissolved U species prior to their quantification in water and biological fluids using Surface Enhanced Raman Scattering (SERS). [4] We contend there is need to develop additional U-specific substrates that might improve the sensitivity and selectivity of such sensing approaches, while also providing insights into dissolved U speciation. Therefore, in addition to improved insights into the mechanism of surface-segregation for the production of functionalized polymer nanofibers, novelty from this study is derived through the identification of specific processes that influence U binding to phosphonate-functionalized polymer membranes under environmentally relevant conditions. Although previous studies have utilized spectroscopic techniques to explore U uptake on minerals, there remains limited understanding on U uptake in complex environmental water matrixes by functionalized polymers. [25,37,38] Thus, identification of the U uptake mechanisms herein will provide a framework to help advance the application of functionalized polymer nanofibers in various settings for U capture and concentration. [39,40].

2. Materials and methods

2.1. Materials

Polyacrylonitrile (PAN, mol wt. 150,000), dimethyl sulfoxide (DMSO), uranyl nitrate ($UO_2(NO_3)_2$ • 6 H_2O), calcium chloride ($CaCl_2$•2 H_2O, ACS grade >99.5%), sodium bicarbonate ($NaHCO_3$, ACS grade >99.7%), gold(III) chloride ($HAuCl_4$0.3 H_2O), 6-mercaptohexanoic acid (6-MHA) were purchased from Sigma Aldrich. For studies with different chain length phosphonate surfactants, octadecyl phosphonic acid (ODPA, 97%), hexadecyl phosphonic acid (HDPA, 97%), tetradecyl phosphonic acid (TDPA, 98%), *n*-dodecyl phosphonic acid (DDPA, 97%) and decyl phosphonic acid (DPA, 97%) were also purchased from Sigma Aldrich and used as received. Sodium hydroxide (NaOH), hydrochloric acid (HCl), nitric acid (HNO_3), and ethanol were purchased from Fisher Scientific. Ultrapure water (18.2 MΩ cm^{-1}) was used to prepare all the reagents. All glassware were cleaned with aqua regia (3:1 HCl/HNO_3) and rinsed with ultrapure water before drying in the oven. *Caution: $UO_2(NO_3)_2$•6 H_2O* contains radioactive ^{238}U, which is an alpha emitter, and like all radioactive materials, must be handled with care. These experiments were conducted by trained personnel in a licensed research facility with special safety precautions taken towards the handling, monitoring, and disposal of radioactive materials.

2.2. Electrospun nanofiber synthesis

Fabrication of the electrospun mat was performed on a custom designed electrospinner as detailed in our previous work. [11,25,41] As an example, the sol-gel for HDPA-functionalized materials was created by dissolving the parent PAN polymer (0.36 g) and HDPA surfactant (0.031 g) into 5 mL of dimethyl sulfoxide (DMSO) solvent. This corresponds to HDPA at 0.5 wt% relative to the overall sol gel mass (and an HDPA mole fraction of 1.44×10^{-3}), which was the optimal loading for HDPA-functionalized materials that we previously reported. [25] For sol gels with other phosphonate surfactants of varying alkyl chain length, sol gels were prepared at the same mole fraction as the optimal HDPA formula (1.44×10^{-3}) so that all resulting nanofibers contained an equivalent amount of phosphonate moieties.

After their assembly, sol gel mixtures were placed on a rotating Thermomixer (Eppendorf) for 12 h at 700 rpm and 60 °C.This sol-gel is fed through a syringe pump at 0.5 mL/hr and at 16–20% relative humidity to an electrospinner needle at 15 kV applied potential. This results in the formation of the electrospun nanofibers that are deposited on a ground collector surface rotating at 550 rpm. The mats were characterized using Electron Microscopy (SEM, Fig. S1) and Infrared spectroscopy (ATR-FTIR, Fig. S2). Surface area and pore volume measurements for select fibers were collected using N_2 Brunauer-Emmett-Teller (BET) sorption isotherm analysis (Quantachrome Nova 1200 Surface Area Analyzer), and all samples were degassed at 300 °C for 3 h prior to analysis.

2.3. Uptake experiments

2.3.1. Influence of phosphonate surfactant chain length on U uptake studies

U uptake experiments with DPA, DDPA, TDPA, HDPA, and ODPA followed procedures from our prior work. [25] All systems contained a 20 mL solution of 1 μM of uranyl nitrate [$UO_2(NO_3)$•6 H_2O] at pH 2 (Milli-Q Ultrapure water adjusted with 5 N HNO_3) and 5 mg of phosphonate-functionalized nanofibers (0.25 g/L sorbent loading). This pH 2 solution was chosen for these experiments because of its relevance to treatment of U-contaminated acid mine drainage, and our prior work showing maximum removal of U^{6+} using HDPA-functionalized materials

in 1 μM total uranium systems. Reactors were allowed to react for 16 h (i.e., the duration we previously as sufficient to achieve sorption equilibrium), at which point the nanofiber mats were removed from solution and analyzed via liquid scintillation counting (LSC). Because we have previously found that surfactants can leach from electrospun nanofibers once submerged in aqueous solution, [11] uptake experiments were conducted both with as synthesized nanofibers and nanofibers that were extensively washed with water prior to reaction. The washing procedure followed that used previously by our group, [11,25] where 5 mg of a functionalized PAN mat was placed in a 50 mL conical vial with 10 mL of Milli-Q Ultrapure water. Vials were then mixed end over end for 24 h, and the water was exchanged three times over that interval.

2.3.2. Mechanism of U uptake studies

Batch experiment were performed to investigate the mechanism of uranium uptake on the polymer mat. The characteristics of spring and surface waters near mine waste sites in New Mexico and Arizona measured in previous studies had pH ranging from 6.8 to 8.2, alkalinity values from 100 to 430 mg/l as $CaCO_3$, Ca^{2+} concentration between 30 and 280 mg/l and U concentration between 50 and 700 μg/l. [1,32,42] Based on these field conditions, we prepared U stock solutions for use in batch uptake experiments. The solutions were prepared in 18.2 MΩ ultrapure water with 10 μM uranyl nitrate [$UO_2(NO_3)$•6 H_2O] at pH 7.0 (buffered with 0.1 M HEPES). Initial uptake experiments were performed by adding 20 mL of the U stock solutions with 5 mg HDPA electrospun polymer mat in a centrifuge tube for 16 h and are referred to throughout this work as *HDPA+U reactor*. Additional experiments were conducted with 10 μM U (uranyl nitrate), (i) 5 mM Ca (as $CaCl_2$) referred as *HDPA+U+Ca* reactor (ii) 5 mM CO_3 (as $NaHCO_3$) (designated *HDPA+U+CO_3* reactor) and (iii) 5 mM each of Ca and CO_3 (*HDPA+U+Ca+CO_3* reactor), together at pH 7.0 (Adjusted with HCl). Upon completion of reaction, the electrospun polymer mat were removed from the reactor, rinsed with deionized water, and prepared for solid analyses.

2.4. Extraction experiments

A set of experiments were conducted to evaluate U release from the polymer mats after the uptake experiments. A subsample of the reacted mats from the uptake experiment reactors were taken for extraction experiments, referred to as *reacted HDPA+U*, *reacted HDPA+U+Ca*, *reacted HDPA+U+CO_3* and *reacted HDPA+U+Ca+CO_3* mats. These mats were reacted with 15 mL of either: (i) 1 M $MgCl_2$ at room temperature at pH 7 for 1 h to extract ion exchangeable species bound to the surface through ionic interactions or outer-sphere complexes, [43,44] or (ii) 50 mM HCO_3 (pH 8.3) to extract adsorbed U as inner sphere and outer sphere surface complexed U. [32,42,45] These extractions were performed on a benchtop mixture rotating at 60 rpm for 12 h.

2.5. Solid and liquid analyses

The top 5 nm (near surface) of reacted and control (unreacted) polymer mats were analyzed using survey and high-resolution X-ray Photoelectron Spectroscopy scans for the spectroscopic features of U, C, O, P and N. This provides insights on the binding chemistry of organic groups with U. The changes in binding environment of U were observed using the U 4 *f* high resolution scan. Spectra were collected from three different areas on each sample using a Kratos Axis DLD Ultra XPS with a Mg Kα source. XPS high resolution spectra was collected for U 4 *f*, C 1 *s*, N 1 *s*, O 1 *s*, and P 2*p* using step size of 0.1 eV and pass energy of 20.

X-ray Absorption Spectroscopy (XAS) analyses were conducted at the Stanford Synchrotron Radiation Lightsource (SSRL) at beam line 11–2 to identify changes in oxidation state (XANES) and molecular coordination (EXAFS) of U during these batch experiments. The EXAFS provides coordination number, and bond distances (eg. U-U, U-N and U-C) in the local molecular environment and help identify the surface complexes when compared to reference values. These references (U adsorbed ferrihydrite, liebigite and carnotite) were analyzed during the same beamtime. At least six scans were collected for each sample, and 3 scans for the references.

Surface Enhanced Raman Scattering (SERS) measurements were collected using a semi-homebuilt Raman microscope (Olympus BX51, Intevac ExamineR 785) with a 10x objective coupled to a solid-state laser with an excitation wavelength of 785 nm, integration time of 40 s, spot size of 10 μm, and power of ~15 mW. Gold nanostars were synthesized and functionalized using a modified protocol from previous papers (SI, text S1). [4,40] Prior to analysis, samples were placed on a glass slide, hydrated using 30 μL ultrapure water, and covered with a cover slip. Light pressure was applied to the cover slip to eliminate trapped air-bubbles. SERS spectra were randomly collected at 8–10 different spots across the mats. These signals were averaged then subtracted using an averaged SERS spectrum collected on HDPA PAN mats (with gold nanostars but without U). Integrated areas from 870 to 806 cm^{-1} were calculated to determine relative abundance of uranyl species on *reacted HDPA+U* and *reacted HDPA+U+Ca* mats. For *reacted HDPA+U+CO_3* and *reacted HDPA+U+Ca+CO_3 reacted*, integrated areas from 852 to 806 cm^{-1} were calculated as SERS signals of uranyl.

For phosphonate alkyl chain length studies, the concentration of U sorbed on functionalized nanofibers at equilibrium was determined via LSC according to the methodologies provided in Johns et al. [25] For all other U uptake studies, a Perkin-Elmer Nexion 300D inductively coupled plasma-mass spectrometer (ICP-MS) system was used to analyze the total U concentration in liquid samples from the reactor. Additionally, chemical equilibrium modelling for U aqueous speciation was carried out using Visual MINTEQ with inputs based on the experimental conditions used for this study.

3. Results and discussion

3.1. Electrospun polymer characterization

The electrospun polymers have a polymeric backbone with the surfactant present on the surface as ligands as confirmed by XPS survey scans (Table 1). The XPS survey scans for the synthesized HDPA (control) electrospun polymers exhibited 1.3% P on the surface and the presence of a peak at 134 eV region representing XPS P 2*p* confirms the presence of phosphonate on the near surface of the electrospun polymer. The ATR-FTIR spectra (SI, Fig. S2) also shows the presence of P-O-H bonding on the HDPA-PAN control mat. The microscopy results (SI, Fig. S1) indicate that the dimensions of the nanofibers were similar for all the control and reacted mats with the width of each nanofibers at 120 nm and these results confirm similar swelling of the fibers as reported previous studies. [9,25].

3.2. Effect of phosphonate alkyl chain length on U uptake

Results of U uptake studies using PAN functionalized with HPA (6), OPA (8), DPA (10), DDPA (12), TDPA (14), HDPA (16) and ODPA (18) are shown in Fig. 1. Data shown for each material was collected with surfactant-functionalized PAN that was washed extensively prior to contact with U-containing solutions. This washing was intentional so as to dislodge any loosely retained surfactant. For these washed materials, U uptake increased with increasing chain length. For all surfactants with alkyl chains less than 14 carbons (i.e., HPA, OPA, DPA, DDPA, and TPA), U uptake was only slightly greater than that observed in control experiments conducted with unfunctionalized PAN (dashed line in Fig. 1). Far greater U uptake was observed for HDPA (~40% of total U in the system) and ODPA (near complete uptake of all U in the system). Notably, from SEM there were no obvious differences in the morphology of these materials (see Fig. S4) that could also be used to rationalize observed trends in U uptake.

For comparison, we also explored U uptake on a select number of

Table 1
XPS survey scans indicating the atomic composition in the near surface.

	C1*s*%	N1*s*%	O1*s*%	P2*p*%	U4*f*%	Na1*s*%	Ca2*p*%
HDPA control	**80.6** ± 0.98	**8.4** ± 2.4	**9.7** ± 3.7	**1.3** ± 0.34	**n.d.**	**n.d.**	**n.d.**
HDPA+U	**79.5** ± 1.1	**12.7** ± 0.37	**6.5** ± 1.3	**0.4** ± 0.05	**0.2** ± 0.04	**0.7** ± 0.09	**n.d.**
HDPA+U+Ca	**78.8** ± 1.0	**12.6** ± 0.6	**7.5** ± 1.2	**0.4** ± 0.06	**0.2** ± 0.03	**0.2** ± 0.05	**0.2** ± 0.04
HDPA+U+CO_3	**79.9** ± 0.3	**14.4** ± 0.81	**4.4** ± 0.5	**0.4** ± 0.01	**0.1** ± 0.01	**0.7** ± 0.07	**n.d.**
HDPA+U+Ca+CO_3	**77.2** ± 0.2	**18.8** ± 0.24	**3.9** ± 0.06	**0.2** ± 0.04	**0.03** ± 0.02	**0.7** ± 0.07	**n.d.**

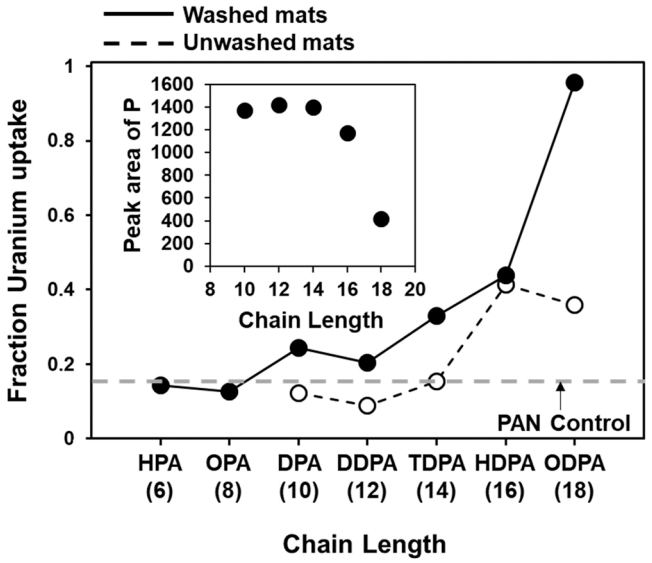

Fig. 1. Effect of alkyl chain length on the fractional uranium (U) uptake by phosphonate-functionalized PAN nanofibers. Data are shown for functionalized nanofibers reacted with 1 μM U at pH 2 in 0.25 g/L sorbent systems for 16 h. Results are shown for materials used immediate after synthesis ("unwashed") and materials used after extensively rinsing with water to remove loosely retained surfactant ("washed"). The U removal observed in control systems with unfunctionalized PAN is shown as a dotted horizontal line. Bracketed numbers along the x-axis indicate the alkyl phosphonate chain length. Error bars, if not visible, are smaller than the symbols. The inset shows the response (based on the P 2p peak area) for P from XPS analysis of unwashed materials (spectra are shown in Fig. S3).

materials that were used in sorption experiments immediately after synthesis (i.e., without washing to remove any loosely retained surfactant). For these unwashed materials, U uptake was less in all cases, with DPA, DDPA, and TPA exhibiting U uptake no greater than that observed in controls with unfunctionalized PAN (dashed line in Fig. 1; note: we presume uptake on unfunctionalized PAN is primarily due to interaction of the uranyl ion with electron-rich cyano groups within the polymer). [17] For unwashed mats containing HDPA and ODPA, U uptake was greater than that observed in controls but equal to (for HDPA) or less than (for ODPA) the degree of sorption observed with the corresponding washed materials.

We have previously found that integration of surfactants into electrospun polymers can promote pollutant uptake via two mechanisms: (i) when well retained inside the polymer (i.e., surfactants retained after washing), charged surfactant head groups present on the nanofiber surface act as complexation sites for dissolved species; and/or (ii) when poorly retained inside the polymer (i.e., surfactants are lost to solution during washing), the release of surfactant into the solution leaves behind pores that can increase the specific surface area of the polymer (i.e., the surfactant acts as a porogen). [11,46] Typically, we have observed the greatest improvements in sorption capacity when the surfactant is well-retained inside the polymer, allowing the charged surfactant head on or near the polymer surface to selectively bind dissolved targets of opposite charge. Increases in uptake resulting from the surfactant acting as a porogen are typically less, but depend on the extent of surface area created by the resulting pore space and the inherent binding activity of the substrate in which the pores are generated.

Based upon these prior experiences with surfactant-functionalized PAN, we attribute the trends in U uptake shown in Fig. 1 to differences in the retention of phosphonate surfactants with different alkyl chain lengths within PAN nanofibers. We postulate that phosphonate surfactants with shorter chain lengths (all those with alkyl chain lengths less than 14-carbon TDPA) are poorly retained in PAN. Upon immersion in aqueous solution, we suspect that their release from PAN is near complete and occurs relatively quickly, consistent with our observation of foaming (indicative of surfactants) within our reactors during U uptake experiments with materials used immediately after synthesis (i.e., unwashed materials). Accordingly, the slight increase in U uptake observed for DPA, DDPA, and TDPA after washing of these materials (see Fig. 1) likely results from increases in pore volume and specific surface area of the PAN that are produced when the surfactant is lost into solution. Indeed, based upon N_2 BET adsorption isotherm analysis, we observed notable increases in the measured pore volumes for HPA (6 carbons) and OPA (8 carbons) after our washing procedure to remove loosely bound surfactant (Table S1), consistent with their roles as porogens. [11].

In contrast for HDPA- and ODPA-functionalized materials, we hypothesize that their longer alkyl chains promote improved retention in the PAN, presumably through increased physical entanglement and hydrophobic interactions between their longer alkyl chains and polymer. This helps to immobilize their phosphonate heads on or near the PAN surface, where they are available to promote U uptake to levels well above those observed for unfunctionalized PAN. This is consistent with the U uptake observed for both unwashed and washed types of these materials, and notably there was no statistically significant increase in pore volume or surface area for ODPA functionalized materials after washing (see Table S1).

Without an observable increase in surface area or pore volume for ODPA-functionalized materials after washing, the increase in U uptake observed for washed ODPA-functionalized nanofibers is not entirely understood. We note that XPS analysis of as synthesized, unwashed materials revealed that surface P concentration was actually lowest for ODPA, with the greatest surface P concentrations measured for materials with shorter chain surfactants (see inset to Fig. 1 and Fig. S3). We are left to speculate that the increase in U uptake on ODPA-functionalized materials after washing may be due to the release of poorly retained ODPA that is loosely bound primarily on the PAN surface rather than the bulk of the material, thereby limiting pore formation. Indeed, we noticed a small degree of foaming during the washing of HDPA- and ODPA-containing materials, indicative that a small portion of surfactant was released into solution during our washing procedure. If primarily bound to the polymer surface, loosely retained ODPA could have an inhibitory effect on uptake of U by unwashed materials by blocking more well-retained phosphonate sites that persist in the washed materials. Such interference of loosely retained, surface-bound ODPA on as synthesized materials could also explain the relatively low surface P concentration measured by XPS on unwashed ODPA-functionalized PAN (with 18 carbon atoms for every one P atom in surface-associated ODPA molecule). For example, the atomic of abundance of P relative to carbon in ODPA ($C_{18}H_{39}O_3P$) is only ~5%, which would be expected to lower the

P 2p intensity measured with XPS. Additional experimental work is necessary, however, to further explore the greater uptake of U on ODPA-functionalized materials after washing.

3.3. Experiments probing U uptake

All subsequent experiments exploring U uptake were conducted using HDPA-functionalized materials. Although ODPA-functionalized materials exhibited more U uptake capacity, it was also more difficult to reproducibly synthesize due to stability issues with the sol gel precursor. We also have previously investigated HDPA-functionalized materials, thus we had a greater understanding of its performance (e.g., pH-dependent U uptake) than ODPA-functionalized materials.

The results from the uptake experiments indicate that the interaction of U with carbonate and with a mixture of calcium and carbonate causes the inhibition of U uptake on the HDPA electrospun polymer. For example, lower U uptake was observed in the *HDPA+U+CO₃* and *HDPA+U+Ca+CO₃* reactors when compared to the reactors without CO_3 (Fig. 2). Comparable U uptake was observed in the *HDPA+U* reactor (1.98 ± 0.07 μg U/mg mat) and in the *HDPA+U+Ca* reactor (1.96 ± 0.37 μg U/mg mat). This similarity in U uptake can be attributed to highly preferential sorption of U on HDPA resulting in limited cationic competition from Ca. [8,47] The uptake in the *HDPA+U+CO₃* reactors was 1.14 ± 0.22 μgU/mg mat, corresponding to 39.4% decrease in U uptake compared to the *HDPA+U* reactor. The *HDPA+U+Ca+CO₃* reactors had the least U uptake (0.35 ± 0.24 μg U/mg mat) which corresponds to 82% decrease when compared to the *HDPA+U* reactor. This decrease is comparable to that observed in other studies showing 70% decrease in U sorption on mineral surfaces when Ca and CO_3 are present. [48,49] Thus, the presence of co-occurring ions influences the U uptake into the HDPA mats, which may be attributed to changes in U aqueous complexation.

The formation of neutral or negatively charged uranyl-carbonate or ternary calcium-uranyl-carbonate aqueous complexes decreases the binding of U in the mats. Chemical equilibrium modelling was used to further interpret the results from the uptake experiments and presented in Fig. S5. Simulations at pH 7 suggest that the cationic U aqueous species are prevalent in the *HDPA+U* reactors and in the *HDPA+U+Ca* reactors, with 70% $(UO_2)_3(OH)_5^+$, 20% $(UO_2)_5(OH)_7^+$ and 6% UO_2OH^+. Anionic U aqueous species are prevalent in the *HDPA+U+CO₃* reactors, with 75% $UO_2(CO_3)_3^{-4}$ and 21% $UO_2(CO_3)_2^{-2}$. For the *HDPA+U+Ca+CO₃* reactors, 67% $Ca_2UO_2(CO_3)_3$ neutral U species and 31% $CaUO_2(CO_3)_3^{-2}$ anionic U species were present. The presence of these ternary calcium-uranyl-carbonate aqueous complexes has also been reported in other studies. [7,34,50] As our experiments are conducted at pH 7 > pK_a= 2.6 for HDPA, the surface is negatively charged, causing electrostatic repulsion with the negative and neutral aqueous complexes. This would prevent U binding with the HDPA surface and resulting in lower uptake for *HDPA+U+CO₃* and *HDPA+U+Ca+CO₃* reactors. Additional extraction experiments with targeted reactants were pursued to better understand the U release to solution from surface associated U species on the reacted mats.

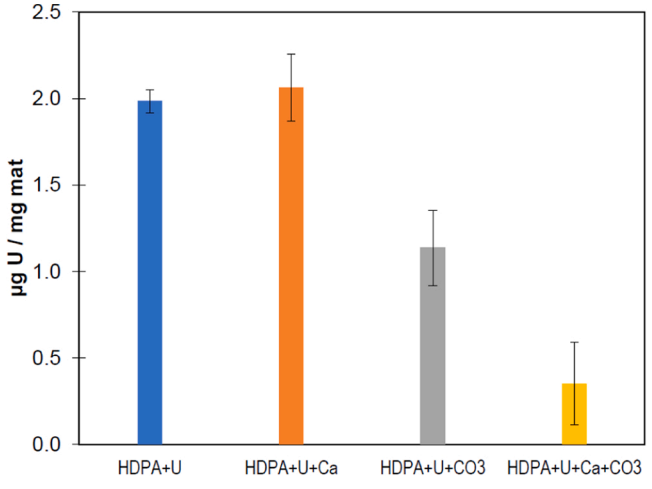

Fig. 2. Uptake of U (μg U / mg mat) on HDPA-PAN electrospun mats reacted with 10 μM [U], 50 mM [HEPES] and in the presence of either 5 mM [Ca] (orange), 5 mM [CO_3] (gray) or both 5 mM [Ca] and [CO_3] (yellow). The experiments were conducted using 5 mg mat in 20 mL solution reacted for 16 h. Error bars represent the standard deviation of triplicate reactors.

3.4. Extractions experiments

Higher U release from the HDPA reacted mats was observed after extractions with HCO_3 compared to $MgCl_2$, indicating that the U associated to these mats is more amenable to complexation rather than ion exchange. The results from the extraction experiments are presented in Fig. 3. The *reacted HDPA+U* mats had 70% higher U release (3.0 μg HCO_3 extractable U) with extractions using HCO_3 when compared to $MgCl_2$ extractions (0.9 μg $MgCl_2$ extractable U). A similar trend was observed for the *reacted HDPA+U+Ca* mats, given that 78% higher HCO_3 extractable U (3.9 μg) was released when compared to $MgCl_2$ extractable U (0.8 μg). An order of magnitude higher HCO_3 extractable U was obtained for the *reacted HDPA+U+CO₃* mats (1.7 μg U) and *reacted HDPA+U+Ca+CO₃ reacted* mats (0.6 μg U) in contrast to that released from $MgCl_2$ extractions (0.02 μg for *reacted HDPA+U+CO₃ reacted* mats and 0.06 μg for *reacted HDPA+U+Ca+CO₃* mats). This result suggests that U is initially complexed to the surface of the HDPA reacted mats after the uptake experiments, but then is removed from the surface and released to solution after complexation with bicarbonate upon extraction at pH 8.3.

Although the *HDPA+U+CO₃* and *HDPA+U+Ca+CO₃* reactors had lower U uptake, most extractable U was amenable to complexation after HCO_3 addition. The low U released after extractions with $MgCl_2$ indicates limited ion exchangeable U in these mats. Strong complexing agents such as HCO_3^- would bind and solubilize most surface associated U complexes [1,42,51] resulting in release of both the inner sphere and outer sphere surface U complexes into solution. Thus, a higher HCO_3^- and low $MgCl_2$ extractible U support the presence of inner-sphere U surface complex on all the reacted mats.

3.5. Solid analyses

Further analyses of the reacted mats were carried out using XAS, XPS and SERS to understand the binding structure of surface associated U. The EXAFS U L-III spectra (Fig. 4) shows that all the reacted mats had a similar shape to each other, with no matches to the reference

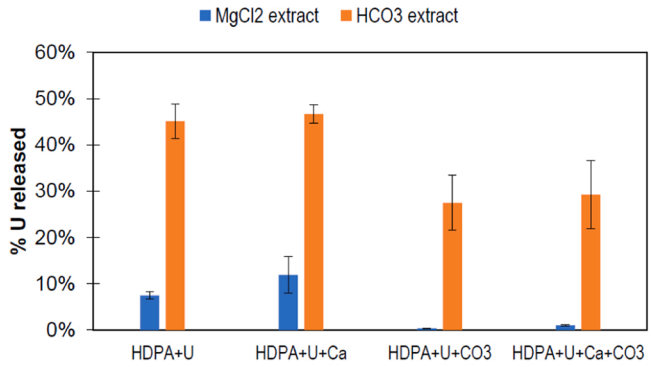

Fig. 3. Results from reactivity experiments indicating % U released from the reacted mats after the addition of extractants (a) $MgCl_2$ (b) HCO_3. Reaction conditions involved taking the reacted mats from U uptake experiments and reacting with each of the extractants.

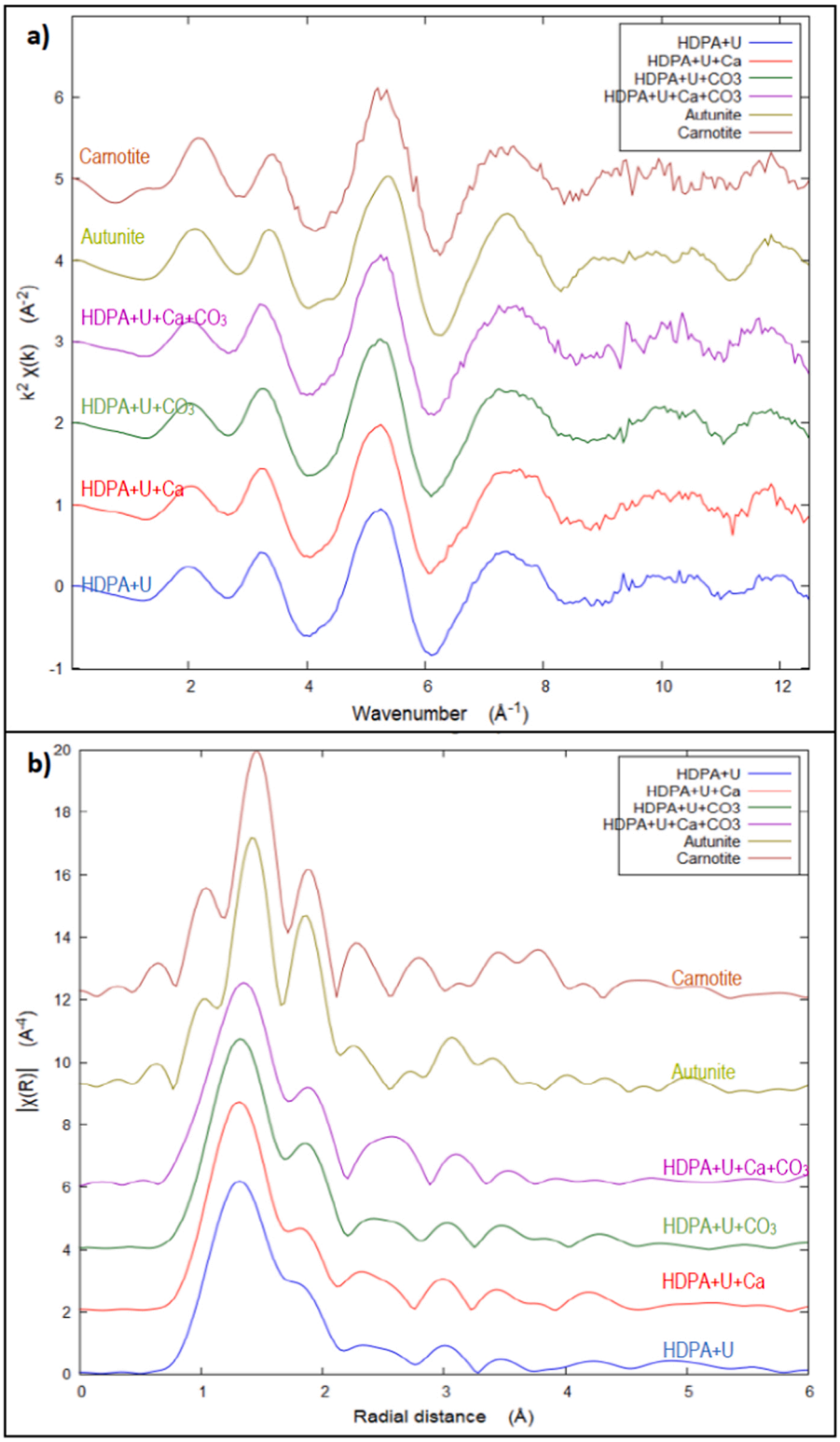

Fig. 4. U LIII-edge EXAFS spectra from beamline 11–2 in (a) real-part (b) Fourier transformed for reacted HDPA mats compared to references autunite and carnotite minerals. Reaction conditions [U] = 10 μM, Mat = 5 mg, volume = 20 mL, pH = 6.8 buffered HEPES = 10 mM.

compounds. To understand the structural motif of the surface associated uranyl, shell-by-shell fitting (Fig. 5) for *reacted HDPA+U mat* was conducted. The fitting of peaks observed in the Fourier Transformed EXAFS spectra (Fig. 4**b,** Fig. 5) around 1.78 Å corresponds to the two U=O dioxo bonds and five U-O bonds with atomic distances of 2.30 Å. The FT peaks at 2.3 Å is likely due to shell of neighboring atoms, which in our system is nitrate ligands, at atomic distance of 2.88 Å. The FT peaks observed from 2.9 to 3.1 Å can be attributed to a second neighbor shell of U-P coordination on HDPA, which suggests inner-sphere complexation through one of the hydroxide of the phosphonic acid functional group (≡P-O-U, atomic distance U-P 3.58 Å). Comparable atomic distances for surface associated U have been reported in literature. [52–54]

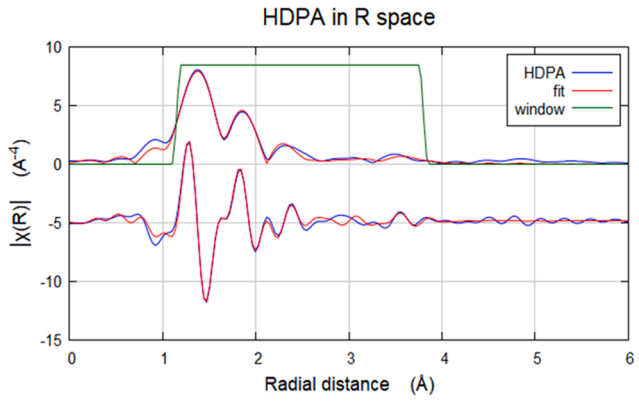

	N, Co-ordination no.	D, distance (Å)	σ^2, mean square deviation (Å^2)
***U-O**axial*	2	1.78(1)	0.0018(1)
***U-O**equatorial*	5	2.30(1)	0.008(1)
U-N	2	2.88(2)	0.003(2)
U-O	2	4.21(3)	0.006(3)
U-P	1	3.58(3)	0.004(3)

Fig. 5. EXAFS shell-by-shell fitting results for HDPA+U mat. Reaction conditions [U] = 10 μM, Mat = 5 mg, volume = 20 mL, pH = 6.8 buffered HEPES = 10 mM.

The similar EXAFS spectra for all other reacted mats (*HDPA+U+Ca, HDPA+U+CO_3, HDPA+U+Ca+CO_3*) indicates that the U binding on surface was consistent to the *HDPA+U* only shell-by-shell fitting. Thus, the U is present as a seven coordinated inner-sphere complex (UO_2O_5) with the HDPA mat as seen from the EXAFS shell-by-shell fitting.

The XPS survey scans and U 4 *f* high-resolution spectra detected the presence of U in the near surface of all the reacted mats (Table 1). The U 4 *f* high resolution spectra for all reacted mats had similar shapes which indicates similar U(VI) binding in the near surface (Fig. 6). Fitting of the U 4 $f_{7/2}$ spectra indicates the presence of two components with binding energy at 381.6 eV and 379.6 eV. A U 4 *f* satellite peak is observed at 384.4 eV. The U $4f_{5/2}$ spectra imitates the shape of the components of U $4f_{7/2}$ with exactly 10.9 eV lower binding energy and one-third of the intensity. [55] Since these two components are present for all the reacted mats, the near surface associated uranyl species is likely the same. Analysis of high-resolution P 2*p* spectra indicate that there are no noticeable changes in shape for all the reacted mats. The lack of changes in the EXAFS U L-III spectra and XPS U 4 *f* high resolution spectra in all the reacted mats suggests that similar binding environment on the surface reacted HDPA mats in all reaction conditions.

SERS measurements with Au-MHA nanostars are utilized to determine uranyl complexes present on HDPA-PAN mat upon coordinating with uranyl and different ions based on molecular vibrational frequencies in the spectra. Fig. 7 shows SERS spectral deconvolution results for *reacted HDPA+U, HDPA+U+Ca, HDPA+U+CO_3* mats suggest the presence of monodentate uranyl phosphonate species. No U signal was observed on *reacted HDPA+U+Ca+CO_3* mats due to the low U uptake on the mats was below the detection limit of SERS. The identity of the associated uranyl complexed are assigned based on known vibrational frequency perturbations from carboxylate (from MHA) and phosphonate (from HDPA). While both functional groups induce a red-shift in the uranyl nitrate frequency, which is typically centered at 870 ± 1 cm^{-1}, each functional group induces a specific red-shift that depends on the ligand denticity and systematic impacts on vibrational feature band width (estimated using full width at half maximum). Previously, it was shown that monodentate (κ^1)coordination to carboxylate and phosphonate groups induce a red shift of 11 cm^{-1} and bidentate (κ^2) carboxylate coordination a 20 cm^{-1} shift. [56] Thus, vibrational frequencies at 859 ± 1, 847 ± 1, 838 ± 1, and 828 ± 1 cm^{-1} are tentatively

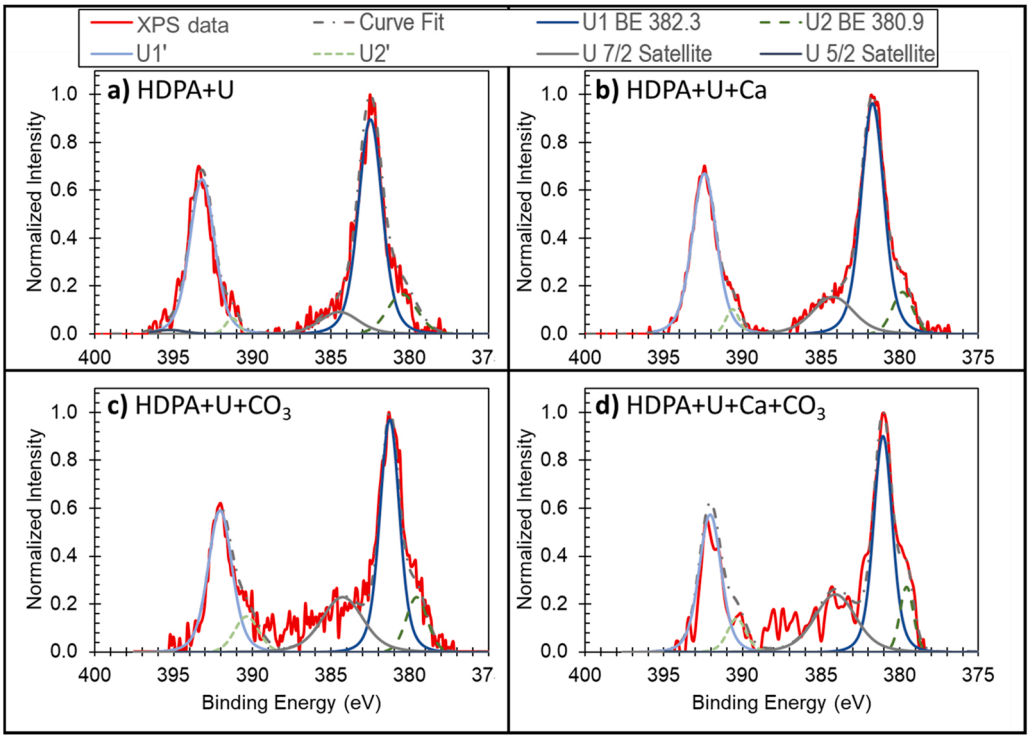

Fig. 6. XPS High Resolution U 4 f photo peak for reacted samples (red) and fittings of U 4 f components (inset) for reacted HDPA mats (a) 10 μM U, (b) 10 μM U+ 5 mM Ca^{2+}, (c) 10 μM U + 5 mM CO_3^{2-} and (d) 10 μM U+ 5 mM Ca^{2+} + 5 mM CO_3^{2-}, from U uptake experiments. Reaction conditions [U] = 10 μM, Mat = 5 mg, volume = 20 mL, pH = 6.8 buffered HEPES = 10 mM.

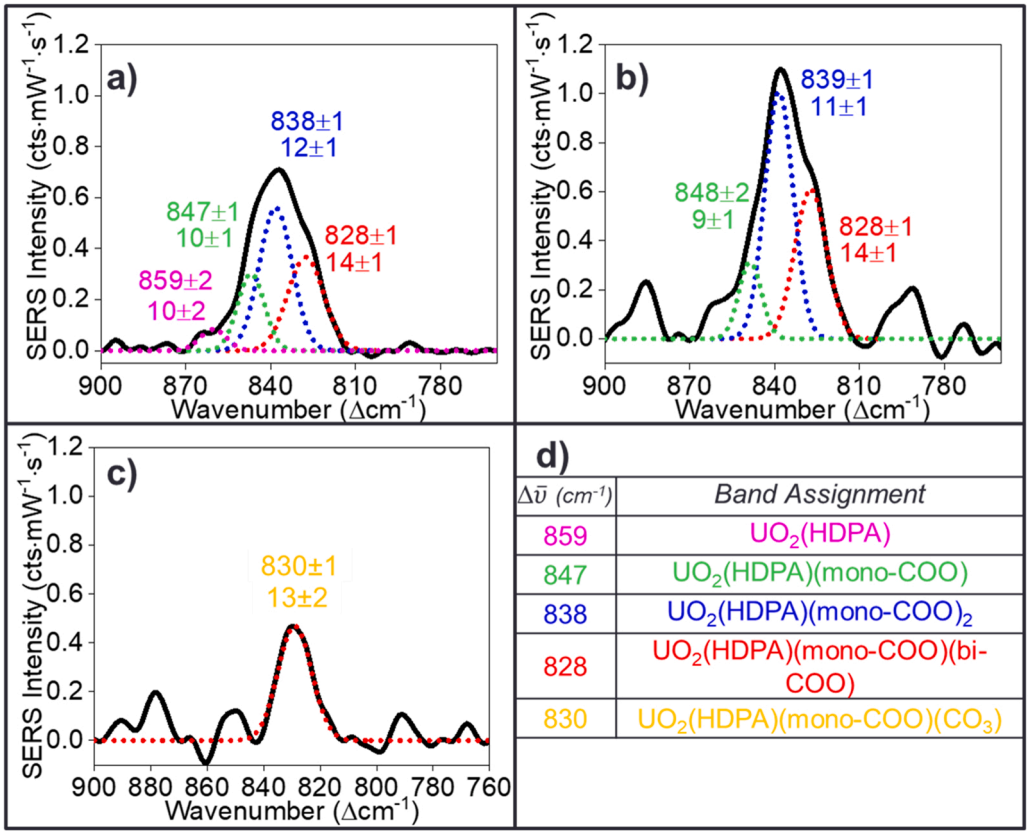

Fig. 7. SERS spectra and deconvolution results on HDPA PAN mats incubated with (a) 10 μM U, (b) 10 μM U+ 5 mM Ca^{2+}, (c) 10 μM U + 5 mM CO_3^{2-} and (d) shows detected uranyl-HDPA complexes matched with vibrational frequencies obtained from the band deconvolution.

assigned as $UO_2(HDPA)(NO_3)_2^-$, $UO_2(HDPA)(\kappa^1\text{-}COO)(NO_3)^-$, $UO_2(HDPA)(\kappa^1\text{-}COO)_2^-$, and $UO_2(HDPA)(\kappa^1\text{-}COO)(\kappa^2\text{-}COO)^-$ complexes, respectively. As a result of the low U uptake in presence of bicarbonate, SERS spectra showed only one feature centered at 829 cm^{-1} for *HDPA+U+CO₃+HDPA* reacted mats, which can be tentatively assigned as $UO_2(HDPA)(\kappa^1\text{-}COO)(\kappa^2\text{-}CO_3)$. These assignments are supported by vibrational feature bandwidths assignments as these are impacted by the number and extent of electron donating ligands at the equatorial plane of uranyl cation. [4,38] Specifically, previous studies [5,57] showed the increased number of ligands causes the vibrational band width to increase by 2 cm^{-1} per ligand. Interestingly on all mat samples, the $UO_2(HDPA)$ complex that was observed via monodentate coordination remained intact despite the presence of nitrate, carboxylate, and carbonate groups. This suggests that the uranyl phosphonate complex has the largest stability constant among uranyl complexes present in solution and on the polymer surface.

3.6. Mechanistic insights

The results from this study indicate that U(VI) binding occurs primarily on the deprotonated oxygen of the phosphonate (≡P-O^-). As the cationic U aqueous species would easily bind to the negatively charged ≡P-O^- surface site, a higher U uptake was observed for the *HDPA+U* and *HDPA+U+Ca* reactors. The lower U uptake in the *HDPA+U+CO₃* and *HDPA+U+Ca+CO₃* reacted mats is due to the repulsion between anionic aqueous U species with the negatively charge phosphonate polymer surface. This limited U-uptake was confirmed by the minimal ion-exchangeable surface complexes. The surface associated U is predominantly an inner-sphere surface complex, as observed from the HCO_3^- extractions and EXAFS solid analyses. Finally, vibrational spectroscopy analysis suggests that U-phosphonate species are the most thermodynamically stable species present on the mats regardless of the initial U solution chemistry. The presence of this strongly complexed U-phosphonate for all the solution conditions indicate selective U uptake as reported in uranium-phosphonates literature. [31,36,58] Thus, the surficial interaction of aqueous U species strongly influences the total U uptake on the solid electrospun polymer.

3.7. Conclusions

Uranium remains a persistent water quality problem for many drinking water consumers reliant on groundwater as a source in the arid southwestern United States. There remain opportunities for technological advances that can improve access to reliable methods for uranium detection and treatment. Outcomes of the current work help to improve our understanding of the fabrication and performance of a promising material class, functionalized electrospun polymers, that could be integrated into sensing and treatment applications. [4,25].

For functionalized polymer fabrication, we find that longer chain alkyl phosphonates perform best for U uptake. We attribute this behavior to their inherent nature to segregate at the air-polymer interface during electrospinning, and, most importantly, their better retention within the polymer nanofiber matrix during application. More work is needed to better understand the nature of the surfactant-polymer interaction responsible for the better retention of HDPA and ODPA, and whether this observation is more broadly applicable to other types of surfactants integrated into other types of electrospun polymers.

Related to phosphonate-functionalized nanofiber polymer performance, the presence of environmentally relevant concentrations of Ca and CO_3 inhibits U uptake in phosphonate functionalized electrospun polymers. Using spectroscopic methods, we identified the mechanism of U uptake as inner-sphere complexation with U-phosphonate monodentate surface complexes, which were observed on all the reacted mats. Ultimately, given their modest uptake, we envision that these

functionalized nanofiber membranes may be better suited for applications in sensing rather than treatment, where the stability of inner-sphere complexation as a binding mechanism will be desirable for highly specific binding in complex environmental or biological matrices.

CRediT authorship contribution statement

Nabil Shaikh: Writing, Conceptualization, Investigation. **Jiajie Qian:** Investigation. **Sewoon Kim:** Investigation and writing. **Hoa Phan:** Investigation and writing. **Juan S. Lezama-Pacheco:** Investigation, Writing, Formal analysis. **Abdul-Mehdi S. Ali:** Investigation, Formal analysis. **David M. Cwiertny:** Supervision, Investigation, Writing, Project administration, Funding acquisition. **Tori Z. Forbes:** Supervision, Investigation, Writing project administration, Finding acquisition. **Amanda J. Haes:** Supervision, Investigation, Writing project administration and finding. **José M. Cerrato:** Supervision, Investigation, Writing project administration and finding.

Declaration of Competing Interest

The authors declare that they have no known competing financial interests or personal relationships that could have appeared to influence the work reported in this paper.

Data Availability

Data will be made available on request.

Acknowledgements

This work was supported by the U.S. National Institute of Environmental Health Science (NIEHS) under award number R01ES027145 and UNM METALS Superfund Research Program Center P42ES025589 and University of Iowa Superfund Research Program Center P42ES013661. The authors would like to acknowledge Margaret E. Carolan for assistance with U uptake experiments and U analysis. We also acknowledge the NIEHS K.C. Donnelly Externship Award Supplement which supported Nabil Shaikh to perform experiments at the University of Iowa. AJH's acknowledges the IR/D (Individual Research and Development) program associated with her appointment at the National Science Foundation. Use of the SSRL Stanford Synchrotron Radiation Lightsource, SLAC National Accelerator Laboratory, is supported by the U.S. Department of Energy, Office of Science, Office of Basic Energy Sciences under Contract No. DE-AC02-76SF00515.

Appendix A. Supporting information

Supplementary data associated with this article can be found in the online version at doi:10.1016/j.jece.2022.108448.

References

[1] S. Avasarala, P.C. Lichtner, A.-M.S. Ali, R. González-Pinzón, J.M. Blake, J. M. Cerrato, Reactive transport of U and V from abandoned uranium mine wastes, Environ. Sci. Technol. 51 (2017) 12385–12393.
[2] M.E. Harmon, J. Lewis, C. Miller, J. Hoover, A.S. Ali, C. Shuey, M. Cajero, S. Lucas, K. Zychowski, B. Pacheco, E. Erdei, S. Ramone, T. Nez, M. Gonzales, M.J. Campen, Residential proximity to abandoned uranium mines and serum inflammatory potential in chronically exposed Navajo communities, J. Expo. Sci. Environ. Epidemiol. 27 (2017) 365–371.
[3] J. Lewis, J. Hoover, D. MacKenzie, Mining and environmental health disparities in native american communities, Curr. Environ. Health Rep. 4 (2017) 130–141.
[4] G. Lu, A.J. Johns, B. Neupane, H.T. Phan, D.M. Cwiertny, T.Z. Forbes, A.J. Haes, Matrix-independent surface-enhanced raman scattering detection of uranyl using electrospun amidoximated polyacrylonitrile mats and gold nanostars, Anal. Chem. 90 (2018) 6766–6772.
[5] G. Lu, A.J. Haes, T.Z. Forbes, Detection and identification of solids, surfaces, and solutions of uranium using vibrational spectroscopy, Coord. Chem. Rev. 374 (2018) 314–344.
[6] P.J. Lebed, J.-D. Savoie, J. Florek, F. Bilodeau, D. Larivière, F. Kleitz, Large pore mesostructured organosilica-phosphonate hybrids as highly efficient and regenerable sorbents for uranium sequestration, Chem. Mater. 24 (2012) 4166–4176.
[7] W. Dong, S.C. Brooks, Determination of the formation constants of ternary complexes of uranyl and carbonate with alkaline earth metals (Mg^{2+}, Ca^{2+}, Sr^{2+}, and Ba^{2+}) using anion exchange method, Environ. Sci. Technol. 40 (2006) 4689–4695.
[8] E.P. Horwitz, M.L. Dietz, R. Chiarizia, H. Diamond, A.M. Essling, D. Graczyk, Separation and preconcentration of uranium from acidic media by extraction chromatography, Anal. Chim. Acta 266 (1992) 25–37.
[9] J. Qian, B. Jennings, David M. Cwiertny, A. Martinez, Emerging investigator series: development and application of polymeric electrospun nanofiber mats as equilibrium-passive sampler media for organic compounds, Environ. Sci. Process. Impacts 19 (2017) 1445–1456.
[10] J.J. Alcaraz-Espinoza, A.E. Chávez-Guajardo, J.C. Medina-Llamas, C.A.S. Andrade, C.P. de Melo, Hierarchical composite polyaniline–(electrospun polystyrene) fibers applied to heavy metal remediation, ACS Appl. Mater. Interfaces 7 (2015) 7231–7240.
[11] K.T. Peter, N.V. Myung, D.M. Cwiertny, Surfactant-assisted fabrication of porous polymeric nanofibers with surface-enriched iron oxide nanoparticles: composite filtration materials for removal of metal cations, Environ. Sci. Nano 5 (2018) 669–681.
[12] L. Hu, X.-W. Yan, C.-G. Yao, S.-Y. Deng, X.-M. Gao, X.-J. Zhang, D. Shan, Preparation of amidoximated coaxial electrospun nanofibers for uranyl uptake and their electrochemical properties, Sep. Purif. Technol. 171 (2016) 44–51.
[13] K.E. Greenstein, N.V. Myung, G.F. Parkin, D.M. Cwiertny, Performance comparison of hematite (α-Fe_2O_3)-polymer composite and core-shell nanofibers as point-of-use filtration platforms for metal sequestration, Water Res. 148 (2019) 492–503.
[14] P. Singhal, B.G. Vats, V. Pulhani, Magnetic nanoparticles for the recovery of uranium from sea water: challenges involved from research to development, J. Ind. Eng. Chem. 90 (2020) 17–35.
[15] P. Singhal, B.G. Vats, A. Yadav, V. Pulhani, Efficient extraction of uranium from environmental samples using phosphoramide functionalized magnetic nanoparticles: understanding adsorption and binding mechanisms, J. Hazard. Mater. 384 (2020), 121353.
[16] K. Yoon, K. Kim, X. Wang, D. Fang, B.S. Hsiao, B. Chu, High flux ultrafiltration membranes based on electrospun nanofibrous PAN scaffolds and chitosan coating, Polymer 47 (2006) 2434–2441.
[17] N. Horzum, T. Shahwan, O. Parlak, M.M. Demir, Synthesis of amidoximated polyacrylonitrile fibers and its application for sorption of aqueous uranyl ions under continuous flow, Chem. Eng. J. 213 (2012) 41–49.
[18] S. Chatterjee, S. De, Adsorptive removal of arsenic from groundwater using a novel high flux polyacrylonitrile (PAN)–laterite mixed matrix ultrafiltration membrane, Environ. Sci. Water Res. Technol. 1 (2015) 227–243.
[19] F. Huang, Y. Xu, S. Liao, D. Yang, Y.-L. Hsieh, Q. Wei, Preparation of amidoxime polyacrylonitrile chelating nanofibers and their application for adsorption of metal ions, Materials 6 (2013) 969–980.
[20] F. Sebesta, J. John, A. Motl and K. Stamberg, Evaluation of polyacrylonitrile (PAN) as a binding polymer for absorbers used to treat liquid radioactive wastes, United States, 1995.
[21] K.J. Gagnon, H.P. Perry, A. Clearfield, Conventional and unconventional metal–organic frameworks based on phosphonate ligands: MOFs and UMOFs, Chem. Rev. 112 (2012) 1034–1054.
[22] J.-G. Mao, Structures and luminescent properties of lanthanide phosphonates, Coord. Chem. Rev. 251 (2007) 1493–1520.
[23] J. Xie, R. Lv, H. Peng, J. Fan, Q. Tao, Y. Dai, Z. Zhang, X. Cao, Y. Liu, Phosphate functionalized poly(vinyl alcohol)/poly(acrylic acid) (PVA/PAA): an electrospinning nanofiber for uranium separation, J. Radioanal. Nucl. Chem. 326 (2020) 475–486.
[24] Z. Zeng, S. Yang, L. Zhang, D. Hua, Phosphonate-functionalized polystyrene microspheres with controlled zeta potential for efficient uranium sorption, RSC Adv. 6 (2016) 74110–74116.
[25] A. Johns, J. Qian, M.E. Carolan, N. Shaikh, A. Peroutka, A. Seeger, J.M. Cerrato, T. Z. Forbes, D.M. Cwiertny, Functionalized electrospun polymer nanofibers for treatment of water contaminated with uranium, Environ. Sci. Water Res. Technol. 6 (2020) 622–634.
[26] J.G. Lundin, P.N. Coneski, P.A. Fulmer, J.H. Wynne, Relationship between surface concentration of amphiphilic quaternary ammonium biocides in electrospun polymer fibers and biocidal activity, React. Funct. Polym. 77 (2014) 39–46.
[27] Z. Piskuła, T. Manszewski, M. Kubicki, S. Lis, The structure and spectroscopic characterization of UO_2^{2+} complexes with tetraethyl methylenediphosphonate in solution and in solid state, J. Mol. Struct. 1011 (2012) 145–148.
[28] S. Vukovic, B.P. Hay, V.S. Bryantsev, Predicting stability constants for uranyl complexes using density functional theory, Inorg. Chem. 54 (2015) 3995–4001.
[29] T.M. Budnyak, A.V. Strizhak, A. Gładysz-Płaska, D. Sternik, I.V. Komarov, D. Kołodyńska, M. Majdan, V. Tertykh, Silica with immobilized phosphinic acid-derivative for uranium extraction, J. Hazard. Mater. 314 (2016) 326–340.
[30] P. Zhou, B.H. Gu, Extraction of oxidized and reduced forms of uranium from contaminated soils: effects of carbonate concentration and pH, Environ. Sci. Technol. 39 (2005) 4435–4440.
[31] J.D. Kubicki, G.P. Halada, P. Jha, B.L. Phillips, Quantum mechanical calculation of aqueuous uranium complexes: carbonate, phosphate, organic and biomolecular species, Chem. Cent. J. 3 (2009) 10.
[32] J.M. Blake, C.L. De Vore, S. Avasarala, A.-M. Ali, C. Roldan, F. Bowers, M.N. Spilde, K. Artyushkova, M.F. Kirk, E. Peterson, L. Rodriguez-Freire, J.M. Cerrato, Uranium

mobility and accumulation along the Rio Paguate, Jackpile Mine in Laguna Pueblo, NM, Environ. Sci. Process. Impacts 19 (2017) 605–621.
[33] Z. Pan, D.E. Giammar, V. Mehta, L.D. Troyer, J.G. Catalano, Z. Wang, Phosphate-induced immobilization of uranium in hanford sediments, Environ. Sci. Technol. 50 (2016) 13486–13494.
[34] G. Bernhard, G. Geipel, T. Reich, V. Brendler, S. Amayri, H. Nitsche, Uranyl(VI) carbonate complex formation: validation of the $C_a2UO_2(CO_3)_{3(aq.)}$ species, Radiochim. Acta 89 (2001) 511–518.
[35] B. Nowack, A.T. Stone, The influence of metal ions on the adsorption of phosphonates onto goethite, Environ. Sci. Technol. 33 (1999) 3627–3633.
[36] B. Nowack, Environmental chemistry of phosphonates, Water Res. 37 (2003) 2533–2546.
[37] D.M. Singer, K. Maher, G.E. Brown, Uranyl–chlorite sorption/desorption: evaluation of different U(VI) sequestration processes, Geochim. Cosmochim. Acta 73 (2009) 5989–6007.
[38] G. Lu, T.Z. Forbes, A.J. Haes, SERS detection of uranyl using functionalized gold nanostars promoted by nanoparticle shape and size, Analyst 141 (2016) 5137–5143.
[39] G. Lu, T.Z. Forbes, A.J. Haes, Evaluating best practices in raman spectral analysis for uranium speciation and relative abundance in aqueous solutions, Anal. Chem. 88 (2016) 773–780.
[40] H.T. Phan, A.J. Haes, Impacts of pH and intermolecular interactions on surface-enhanced raman scattering chemical enhancements, J. Phys. Chem. C. 122 (2018) 14846–14856.
[41] D.V. Kravchuk, A. Blanes Diaz, M.E. Carolan, E.A. Mpundu, D.M. Cwiertny, T. Z. Forbes, Uranyl speciation on the surface of amidoximated polyacrylonitrile mats, Inorg. Chem. 59 (2020) 8134–8145.
[42] J.M. Blake, S. Avasarala, K. Artyushkova, A.-M.S. Ali, A.J. Brearley, C. Shuey, W. P. Robinson, C. Nez, S. Bill, J. Lewis, C. Hirani, J.S.L. Pacheco, J.M. Cerrato, Elevated concentrations of U and Co-occurring metals in abandoned mine wastes in a northeastern arizona native american community, Environ. Sci. Technol. 49 (2015) 8506–8514.
[43] A. Tessier, P.G.C. Campbell, M. Bisson, Sequential extraction procedure for the speciation of particulate trace metals, Anal. Chem. 51 (1979) 844–851.
[44] T.P. O'Connor, D.R. Kester, Adsorption of copper and cobalt from fresh and marine systems, Geochim. Cosmochim. Acta 39 (1975) 1531–1543.
[45] D.A. Elias, J.M. Senko, L.R. Krumholz, A procedure for quantitation of total oxidized uranium for bioremediation studies, J. Microbiol. Methods 53 (2003) 343–353.
[46] K.T. Peter, A.J. Johns, N.V. Myung, D.M. Cwiertny, Functionalized polymer-iron oxide hybrid nanofibers: electrospun filtration devices for metal oxyanion removal, Water Res. 117 (2017) 207–217.
[47] Y.-L. Wang, L. Zhu, B.-L. Guo, S.-W. Chen, W.-S. Wu, Mesoporous silica SBA-15 functionalized with phosphonate derivatives for uranium uptake, N. J. Chem. 38 (2014) 3853–3861.
[48] A. Kowal-Fouchard, R. Drot, E. Simoni, J.J. Ehrhardt, Use of spectroscopic techniques for uranium(vi)/montmorillonite interaction modeling, Environ. Sci. Technol. 38 (2004) 1399–1407.
[49] C. Tournassat, R.M. Tinnacher, S. Grangeon, J.A. Davis, Modeling uranium(VI) adsorption onto montmorillonite under varying carbonate concentrations: a surface complexation model accounting for the spillover effect on surface potential, Geochim. Cosmochim. Acta 220 (2018) 291–308.
[50] A.S. Saleh, J.-Y. Lee, Y. Jo, J.-I. Yun, Uranium(VI) sorption complexes on silica in the presence of calcium and carbonate, J. Environ. Radioact. 182 (2018) 63–69.
[51] J.M. Blake, S. Avasarala, A.-M.S. Ali, M. Spilde, J.S. Lezama-Pacheco, D. Latta, K. Artyushkova, A.G. Ilgen, C. Shuey, C. Nez, J.M. Cerrato, Reactivity of As and U co-occurring in Mine Wastes in northeastern Arizona, Chem. Geol. 522 (2019) 26–37.
[52] J.R. Bargar, R. Reitmeyer, J.J. Lenhart, J.A. Davis, Characterization of U(VI)-carbonato ternary complexes on hematite: EXAFS and electrophoretic mobility measurements, Geochim. Cosmochim. Acta 64 (2000) 2737–2749.
[53] S. Rihs, C. Gaillard, T. Reich, S.J. Kohler, Uranyl sorption onto birnessite: a surface complexation modeling and EXAFS study, Chem. Geol. 373 (2014) 59–70.
[54] H.A. Thompson, G.E. Brown, G.A. Parks, XAFS spectroscopic study of uranyl coordination in solids and aqueous solution, Am. Mineral. 82 (1997) 483–496.
[55] E.S. Ilton, P.S. Bagus, XPS determination of uranium oxidation states, Surf. Interface Anal. 43 (2011) 1549–1560.
[56] F. Quilès, A. Burneau, Infrared and Raman spectroscopic study of uranyl complexes: hydroxide and acetate derivatives in aqueous solution, Vib. Spectrosc. 18 (1998) 61–75.
[57] C. Ruan, W. Luo, W. Wang, B. Gu, Surface-enhanced Raman spectroscopy for uranium detection and analysis in environmental samples, Anal. Chim. Acta 605 (2007) 80–86.
[58] W. Yang, T.G. Parker, Z.-M. Sun, Structural chemistry of uranium phosphonates, Coord. Chem. Rev. 303 (2015) 86–109.